AIAA SciTech Forum
January 3-7, 2022, San Diego, CA & Virtual
AIAA SCITECH 2022 Forum

10.2514/6.2022-2115

A Macroscopic View of Reynolds Scaling and Stretch Effects in Spherical Turbulent Premixed Flames

Aditya Vinod*, Tejas Kulkarni† and Fabrizio Bisetti‡
Department of Aerospace Engineering and Engineering Mechanics
The University of Texas at Austin
Austin, TX 78712, USA

The burning rate in a spherically turbulent premixed flame is explored using direct numerical simulations, and a model of ordinary differential equations is proposed. The numerical dataset, from a previous work, is obtained from direct numerical simulations of confined spherical flames in isotropic turbulence over a range of Reynolds numbers. We begin the derivation of the model with an equation for the burning rate for the domain under consideration, and using a thin flame assumption and a two-fluid approach, we find the normalized turbulent burning rate to be controlled by the increase in flame surface area due to turbulent wrinkling, and correction factor which is observed to be consistently less than unity. A Reynolds scaling hypothesis for the flame turbulent wrinkling from a previous work using the same numerical dataset is used to model the term controlling the increase in flame surface area. The correction factor is hypothesized to reflect flame stretch effects, and hence this factor is modeled using Markstein theory applied to global averaged quantities. The ordinary differential equations are rewritten to reflect easily observable quantities such as the chamber pressure and mean flame radius, and then expressed in dimensionless form to assess dependence on various dimensionless parameters. The model predictions are found to be in good agreement with the numerical data within expected variances. Additionally, Markstein theory is found to be sufficient in describing the effects of flame stretch in the turbulent premixed flames under consideration.

I. Introduction

Most combustion devices operate with turbulent flow conditions in order to improve power densities through increased burning rates of reactive mixtures. For the most part, this enhancement is brought by increasing flame surface and is customarily quantified by the ratio of the burning rate, i.e. the mass-based rate of fuel consumption in a turbulent flame, to the burning rate of a flame with a suitably defined reference area, burning as a laminar flame. The ratio is often expressed as S_T/S_L, where S_T is the turbulent flame speed and S_L the nominal reference laminar flame speed.

Leveraging an extensive database from Direct Numerical Simulations (DNS), Kulkarni et al. [1–3] proposed a scaling based on the Reynolds number in the form of a power-law for the wrinkling length scale in turbulent spherical turbulent premixed flames subject to decaying turbulence. The proposed scaling implies that the turbulent flame surface area increases with the Reynolds number with power-law exponent close to 0.5, all other parameters held constant.

In Refs. [1–3], the proposed Reynolds scaling was shown to require a correction factor of order unity, but the authors did not provide an explanation for the observed behavior. This work seeks to identify the mechanism responsible for a non-unity correction factor, propose a model, and combine the model with a system of ordinary differential equations (ODEs). The solution to the ODEs describes the evolution of the mean radius and burning rate of the turbulent spherical flame as it propagates outward into the reactants.

The correction factor introduced by Kulkarni et al. [1–3] is defined analogously to the "stretch-factor" discussed in Ref. [4]. A turbulent flame is subject to significant stretch brought by the turbulent velocity field and departures from unity have been attributed to the effect of stretch on the flame displacement speed. Consistent with such postulate, the effect of stretch on the flame speed is often modeled with Markstein theory [5], a linear model for flame stretch effects in steady laminar flames [6]. Extending the Markstein linear model to turbulence, however, is not trivial and the applicability of a linear theory for steady laminar flames to turbulence remains questionable [4]. Nonetheless, such

*Graduate Research Assistant (Corresponding Author: vinoda@utexas.edu)
†Graduate Research Assistant
‡Assistant Professor

Table 1 Simulation parameters at the initial state.

	R1	R2	R3	R4
Symbol	○	□	◇	△
N	512^3	1024^3	2048^3	1728^3
R_0/R_L	0.2015	0.1511	0.1012	0.2015
u'/S_L^0	7.4	8.5	9.8	11.21
l/δ_L^0	3.4	5.2	7.8	12.14
δ_L^0/η	11.3	11.3	11.5	11.2
Re_λ	44	59	77	102
Ka	25	25	25	24.4
n	1.58	1.58	1.71	1.81

an approach is supported by observations in experiments on lean CH_4-air premixed flames [7, 8], which have shown that the thermo-diffusive effects that are modeled in the Markstein-flame-stretch model are present even for Karlovitz number, $Ka > 20$. Several DNS studies [9, 10] have also shown similar results, and have also shown that an effective Markstein number obtained from processing turbulent flame data, $\mathcal{M}_F$, behaves similarly to $\mathcal{M}$ for both stable and unstable flames.

While acknowledging that recent work on turbulent premixed Bunsen flames has put forth alternative explanations for the occurrence of a non-unity correction factor [11], in this work we apply the linear Markstein theory to the modeling of the correction factor. Together with the postulated Reynolds number scaling for the wrinkling scale and additional data from DNS, we formulate a system of ordinary differential equation that, when solved in time, provides an estimate for macroscopic observables such as the mean flame radius, burning rate, and pressure rise in the closed vessel. We expect that the differential model will find application in the post-processing of data from experiments on turbulent spherical premixed flames in closed combustion vessels.

In Section §II the DNS database and flame configuration used in this work are discussed. In Section §III the mathematical model consisting of a set of ordinary differential equations and suitable closures is derived and manipulated in dimensionless form. In Section §IV, the solutions obtained integrating the proposed model are compared against data from Direct Numerical Simulation and the sensitivity of the solutions to non-dimensional parameters is explored with particular emphasis on the Markstein number.

II. Numerical methods

We consider four direct numerical simulations (DNS) of spherical flames subjected to freely decaying homogeneous isotropic turbulence (HIT). A brief description of these simulations is provided below. For more details on the simulations, the reader is directed to our previous work [1].

The unsteady, reactive Navier-Stokes equations are solved in the low Mach number limit with the finite difference solver NGA [12]. The computational domain is cubic with periodic boundary conditions in all three directions. The domain is initialized with CH_4-air gaseous reactant mixture of equivalence ratio $\phi = 0.7$ at initial pressure $p_0 = 4$ atm and temperature $T_{u,0} = 800$ K. The velocity field is initialized as homogeneous isotropic turbulence (HIT) of varying Reynolds numbers, as listed in Table 1 along with other relevant parameters. The chemical reactions are modeled using a kinetics model consisting of 16 species and 73 elementary Arrhenius reactions obtained from GRI-mech 3.0 [13] with mixture-averaged transport properties. The grid spacing is homogeneous for all configurations with $\Delta = 2 \times 10^{-5}$ m, which ensures sufficient resolution of the turbulence spectrum with $\Delta/\eta \leq 0.5$, where η is the Kolmogorov length scale. This grid is such that $\delta_L^0/\Delta = 5.5$, where δ_L^0 is the laminar flame thickness for an unstretched flame at the initial conditions. This resolution has been shown to be adequate for identical thermo-chemical conditions by Luca et al. [14].

Four configurations, named 'R1', 'R2', 'R3' and 'R4', are setup with varying ratios of velocity scales, u'/S_L^0, length scales, l/δ_L^0, and Taylor microscale Reynolds numbers, $\mathrm{Re}_\lambda = u'\lambda/\nu$. Here, $l = u'^3/\epsilon$ is the integral length scale of turbulence, estimated using the turbulence intensity, u', and the mean dissipation rate, ϵ, of the turbulence kinetic energy, k. The Karlovitz number, $\mathrm{Ka} = \tau_L^0/\tau_\eta = 25$, is kept constant across all four configurations, where τ_L^0 and

$\tau_\eta = (\nu/\epsilon)^{1/2}$ are the characteristic laminar flame and Kolmogorov time scales at initial conditions, respectively. This implies that all four simulations lie in the flamelet regime of turbulent combustion [15].

The laminar flame reference scales are calculated used 1D laminar flame calculations. The laminar flame time scale is defined as $\tau_L^0 = \delta_L^0/S_L^0$, where the laminar flame thickness, δ_L^0, and laminar flames speed, S_L^0, are defined at initial time for an unstretched planar laminar flame and are constant across simulations: The laminar flame speed is $S_L^0 = 1.04$ m/s and the laminar flame thickness is $\delta_L^0 = 0.11$ mm, where the laminar flame thickness is defined as a thermal thickness, $\delta_L^0 = (T_{\max} - T_{\min})/\max(|\nabla T|)$.

The flame is initialized as a spherical kernel of products of radius R_0, at the center of the domain. The ratio of the initial flame radius to the equivalent spherical radius of the domain, $R_L = 2L(3/4\pi)^{1/3}$, is adjusted to ensure that the initial flame kernel is large in relation to the integral length scale, l.

All relevant statistics are spherically symmetric and are functions of the radial coordinate, r, and time, t, only. Exploiting this symmetry, statistics are gathered over spherical shells from a single realization. Due to the large R/l ratio, this ensures collection of multiple independent and identically distributed samples, and in turn adequate convergence of statistics.

The free decay of isotropic turbulence in the reactants is found to follow a power law decay [16–18] for the turbulence kinetic energy, k, as

$$k/k_0 = (1 + t/t_0)^{-n} = \exp(-ns), \tag{1}$$

where n and t_0 are the exponent and virtual origin of decay, respectively. The linear time coordinate, t, is transformed into a logarithmic time coordinate, $s = \log(1 + t/t_0)$. The parameters n and t_0 are calculated from the eddy turnover time, $\tau = (t + t_0)/n = k/\epsilon$, using a least squares fit and fall in the range $1.58 \leq n \leq 1.81$.

For purposes of later analysis, we use the mass fraction of oxygen, Y_{O_2}, to define a flame progress variable, $C = (Y_{O_2} - Y_{O_2,b})/(Y_{O_2,u} - Y_{O_2,b})$. Also, the flame is defined as an isosurface of $C(\mathbf{x}, t) = C^*$, and C^* is chosen to be the location of the peak heat release rate in a 1D flame, calculated to be $C^* = 0.73$ for the reactive mixture under study.

III. Mathematical model

This section covers the formulation of the model for the turbulent burning rate, dm_b/dt, eventually obtaining ordinary differential equations (ODEs) that describe observable macroscopic properties of interest in a confined flame in decaying turbulence, such as the mean flame radius, R, the chamber pressure, p. We discuss the assumptions and models used to close these equations and then present them in dimensionless form.

In this work, the " $\wedge$ " accent over symbols is used to represent dimensionless quantities. Subscripts "u" and "b" are used to represent quantities in the reactants and products, respectively, and the superscript "0" on laminar flame properties is used to indicate the corresponding quantity is representative of an unstretched steady laminar flame.

A. Surface Density Function formalism

We assume the turbulent flame to be a thin interface separating reactants and products, in accordance to the Bray-Moss-Libby model [19, 20]. The progress variable, $C(\mathbf{x}, t)$, is a scalar that characterizes the mass fraction of products at a given position and time, equaling 0 in the reactants, 1 in the products and increasing monotonically from 0 to 1 across the flame.

The chamber is assumed to be a sphere of radius, R_L, and this size controls confinement effects on the system. Additionally, all pertinent quantities are ergodic in the azimuthal and polar directions due to spherical symmetry and are functions of radial position, r, and time, t, alone.

The flame surface itself can be characterized by its Surface Density Function (SDF) [21, 22], Σ, defined as the expectation of the flame surface area per unit volume. It is expressed formally in terms of the progress variable field as

$$\Sigma(r, t) = \langle |\nabla C| \delta(C - C^*) \rangle = \langle |\nabla C| | C = C^* \rangle \mathcal{P}_C(C = C^*; r, t), \tag{2}$$

where $\delta(C - C^*)$ is the Dirac delta function operating on $C - C^*$, and $\mathcal{P}_C(C = C^*; r, t)$ is the PDF of the progress variable field. Here C^* defines the flame location, i.e. $C = C^*$ at the flame. It should be noted here that the SDF is a statistic and cannot be defined instantaneously. We also define $\mathcal{P}_r(r; t)$ as the probability density function (PDF) of the radial location of the flame.

Under this formalism, we define the mean flame surface area, A, as

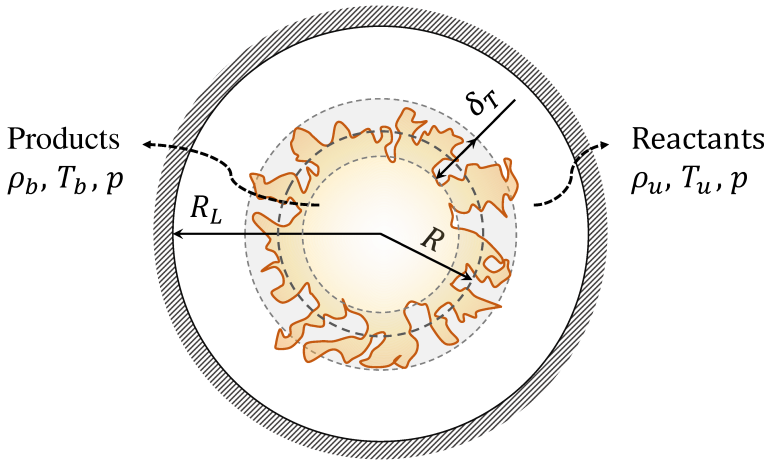

Fig. 1 The chamber setup assumed for a confined spherical turbulent premixed flame.

$$A = 4\pi \int_{r=0}^{\infty} r^2 \Sigma(r,t) dr, \tag{3}$$

the mean flame radius, R, as

$$R(t) = 4\pi A^{-1} \int_{r=0}^{\infty} r^3 \Sigma(r,t) dr = \int_{r=0}^{\infty} r \mathcal{P}_r(r;t) dr, \tag{4}$$

and flame brush thickness, δ_T, as

$$\delta_T(t)^2 = 8\pi^2 A^{-1} \int_{r=0}^{\infty} r^2 (r-R)^2 \Sigma(r,t) dr = 2\pi \int_{r=0}^{\infty} (r-R)^2 \mathcal{P}_r(r;t) dr. \tag{5}$$

For $\delta_T / R << 1$, R can be approximated as the radius, R_b, of a equivalent sphere having the same volume as that of the products, i.e. $R \approx R_b = ((3/4\pi)(m_b/\rho_b))^{1/3}$. Refer to Appendix .A for the derivation of this approximation.

B. Governing equation for the burning rate

The burning rate is defined here as the rate of product mass generation, dm_b/dt. Assuming a flame of negligible thickness, the product mass, m_b, can be defined instantaneously as the mass contained in the region where $C > C^*$. This allows the mass of products to be expressed as an integral of the fluid density over volumes with $C > C^*$.

$$m_b = \iiint_V \rho H(C - C^*) dV. \tag{6}$$

Starting from Eq. (6), expand the burning rate as

$$\frac{dm_b}{dt} = \frac{d}{dt} \iiint_V \rho H(C - C^*) dV = \iiint_V \left(\frac{\partial \rho}{\partial t}\right) H(C - C^*) dV + \iiint_V \rho \frac{\partial}{\partial t} H(C - C^*) dV, \tag{7}$$

where $H(C - C^*)$ is the Heaviside function operating on $C - C^*$. Since the chamber volume, V, is constant, the derivative enters the integral. We simplify the first term in the above expression using the equation of continuity and the divergence theorem.

$$\iiint_V \left(\frac{\partial \rho}{\partial t}\right) H(C-C^*)dV = -\iiint_V \nabla\cdot(\rho\mathbf{u})H(C-C^*)dV \tag{8}$$

$$= -\iiint_V \nabla\cdot(\rho\mathbf{u}H(C-C^*))dV + \iiint_V \rho\mathbf{u}\cdot\nabla H(C-C^*)dV \tag{9}$$

$$= -\oiint_{A_d} \rho\cancelto{0}{H(C-C^*)}\mathbf{u}\cdot\mathbf{n}_d dA_d + \iiint_V \rho\mathbf{u}\cdot\nabla H(C-C^*)dV. \tag{10}$$

The first term in Eq. (10) is an integral over the chamber boundaries, and equals zero under the assumption that $C - C^* < 0$, i.e. the boundaries of the chamber are away from the products. This simplification allows us to combine the derivative in the two terms on the right hand side of Eq. (7) as a material derivative of the Heaviside function, $H(C - C^*)$.

$$\frac{dm_b}{dt} = \iiint_V \rho\frac{D}{Dt}H(C-C^*)dV = \iiint_V \rho\left(\frac{1}{|\nabla C|}\frac{DC}{Dt}\right)_{C=C^*}|\nabla C|\delta(C-C^*)dV. \tag{11}$$

The flame is defined as a propagating interface. Its displacement speed, S, relative to local fluid velocity is defined in terms of the progress variable field, $C(\mathbf{x}, t)$, as [21, 23]

$$S = \left[\frac{1}{|\nabla C|}\frac{DC}{Dt}\right]_{C=C^*}. \tag{12}$$

Using this definition, we rewrite the burning rate as

$$\frac{dm_b}{dt} = \iiint_V \rho S|\nabla C|\delta(C-C^*)dV. \tag{13}$$

We expand the volume integral in spherical coordinates, express the integrand as a statistic and integrate in the ergodic directions, θ and ϕ, to obtain

$$\frac{dm_b}{dt} = \int_{r=0}^{R_L} \langle\rho S|\nabla C||C=C^*\rangle\mathcal{P}_C(C=C^*)r^2dr \int_{\theta=-\pi/2}^{\pi/2} d\theta \int_{\phi=0}^{2\pi} d\phi \tag{14}$$

$$= \int_{r=0}^{R_L} \langle\rho S|\nabla C||C=C^*\rangle\mathcal{P}_C(C=C^*)4\pi r^2dr. \tag{15}$$

We define an area-weighted ensemble average, $\langle\cdot\rangle_w$, and a global average, $\langle\!\langle\cdot\rangle\!\rangle_A$, respectively, as

$$\langle\cdot\rangle_w = \frac{\langle\cdot|\nabla C||C=C^*\rangle}{\langle|\nabla C||C=C^*\rangle}, \tag{16}$$

$$\langle\!\langle . \rangle\!\rangle_A = 4\pi A^{-1}\int_{r=0}^{\infty}\langle . \rangle_w \Sigma r^2 dr = \int_{r=0}^{\infty}\langle . \rangle_w \mathcal{P}_r dr. \tag{17}$$

Using these definitions, and the expression for the SDF, the burning rate reads

$$\frac{dm_b}{dt} = \int_{r=0}^{\infty}\langle\rho S\rangle_w \Sigma 4\pi r^2 dr = A\int_{r=0}^{\infty}\langle\rho S\rangle_w \mathcal{P}_r dr = A\langle\!\langle\rho S\rangle\!\rangle_A. \tag{18}$$

We assume that the density, ρ, is a function of C alone, even within the flame, which allows us to write $\langle\!\langle\rho S\rangle\!\rangle_A = \rho^*\langle\!\langle S\rangle\!\rangle_A$, where $\rho^* = \rho(C = C^*)$. Additionally, we define a reference area, $A^* = 4\pi R^2$, which is the surface area of a

sphere of radius, R. For an unstretched laminar flame of this reference area, the burning rate would be $\rho_u S_L^0 A^*$. Using these we rewrite Eq. 18 as

$$\frac{dm_b/dt}{\rho_u S_L^0 A^*} = \left(\frac{\rho^* \langle\!\langle S \rangle\!\rangle_A}{\rho_u S_L^0}\right)\left(\frac{A}{A^*}\right) = \mathcal{I}\chi, \tag{19}$$

where ρ_u is the reactant density. Here, we define two important factors, $\mathcal{I} = \rho^* \langle\!\langle S \rangle\!\rangle_A / \rho_u S_L^0$ and $\chi = A/A^*$. The area ratio, χ, accounts for the effect of increased surface area of the reactive interface due to turbulent wrinkling. $\mathcal{I}$ is a correction factor, which will be explored further in §III.E.

C. Alternate form of the governing ODE

The governing equation for the burning rate, dm_b/dt, as derived in the previous section reads

$$\frac{dm_b}{dt} = \rho_u A^* S_L^0 \mathcal{I}\chi = 4\pi R^2 \rho_u \chi \mathcal{I} S_L^0. \tag{20}$$

Assuming a homogeneous product density field, we use $m_b \approx (4\pi/3)\rho_b R^3$ to write an ODE for the mean flame radius, R:

$$\frac{dR}{dt} = \left(\frac{\rho_u}{\rho_b}\right)\chi \mathcal{I} S_L^0 - \frac{R}{3}\left(\frac{1}{\rho_b}\frac{d\rho_b}{dt}\right). \tag{21}$$

The burnt mass, m_b, is not easily measured and is hence not a preferred macroscopic quantity. The chamber pressure, p, however is a much more attractive quantity due to its ease of measurement. The pressure rise in a confined combustion chamber is linearly related to the burnt mass fraction, $Y_b = m_b/m$, as [24, 25]

$$Y_b = \frac{p - p_i}{p_f - p_i}, \tag{22}$$

where m is the total mass contained in the chamber, p_f and p_i are the pressures at the fully burnt and unburnt states.

The simplicity of this model (Eq. 22) makes it very attractive for modeling purposes. Equation 22 allows us to rewrite of the ODE for the burnt mass (Eq. (20)) as an ODE for the the chamber pressure, p, as

$$\frac{dp}{dt} = 3\chi \mathcal{I} S_L^0 \left(\frac{1}{R_L^3}\right)\Delta_p R^2 \left(\frac{\rho_u}{\rho_{u,0}}\right), \tag{23}$$

where $\Delta_p = p_f - p_i$, and $\rho_{u,0}$ is the initial reactant density. We also assume isentropic compression of the reactants and products as the flame propagates. The theoretical isentropic expansion factors for the products and reactants, γ_b and γ_u, respectively, are obtained from calculations in Cantera [26]. For the mixture under study, we have $\gamma_u = 1.32$ and $\gamma_b = 1.26$. Letting $Y_b = m_b/m \approx (\rho_b/\rho_{u,0})(R/R_L)^3$ and substituting the equations for isentropic compression of the reactants and products, Eq. (23) is modified to obtain

$$\frac{dp}{dt} = 3\chi \mathcal{I}\left(\frac{S_L^0}{R_L}\right)\Delta_p^{1/3}\sigma^{2/3}(p - p_i)^{2/3}\left(\frac{p}{p_0}\right)^{1/\gamma_u - 2/3\gamma_b}, \tag{24}$$

where $\sigma = \rho_u/\rho_b$ is the density ratio. It should be noted here that p_i/p_0 is not necessarily unity, as the gas at the initial state, $t = 0$, is not assumed unburnt everywhere in the chamber. This complexity is present to accommodate the DNS simulation, which is initialized at $t = 0$ with a spherical kernel of burnt gases at the center, i.e. $Y_b(t = 0) \neq 0$. The unburnt pressure, p_i, is calculated for the such cases using Cantera.

We express the ODEs for R and p in dimensionless form to explore dependencies of the the properties under study on parameters of the gaseous mixture, turbulence and confinement. We use the following reference scales:

- $\rho_{u,0}$, the unburnt gas density at $t = 0$,
- p_0, the chamber pressure at $t = 0$,
- l_0, the integral length scale of turbulence at $t = 0$ and
- τ_0 the eddy turnover time at $t = 0$.

We also rewrite these ODEs in terms of the logarithmic time scale, s.

The dimensionless form of Eq. (21) expressed in s-space reads

$$\frac{d\hat{R}}{ds} = \sigma n \exp(s)\chi\mathcal{I}\hat{S}_L^0 - \frac{\hat{R}}{3\gamma_b\hat{p}}\left(\frac{d\hat{p}}{ds}\right), \tag{25}$$

where the density ratio, σ, is nearly constant over the range of pressures considered. Manipulating Eq. (24), we also write the dimensionless ODE for pressure in s-space as

$$\frac{d\hat{p}}{ds} = 3C_1 n \exp(s)\chi\mathcal{I}\hat{S}_L^0\hat{\Delta}_p^{1/3}\sigma^{2/3}(\hat{p}-\hat{p}_i)^{2/3}\hat{p}^{1/\gamma_u - 2/3\gamma_b}, \tag{26}$$

where $C_1 = l_0/R_L$ is the ratio of the initial integral length scale to the domain size.

We require closures for χ and $\mathcal{I}$. In §III.D we model χ using a Reynolds number scaling hypothesis and §III.E explores the application of laminar flame stretch theory to $\mathcal{I}$.

D. Reynolds Number Scaling of the Area Ratio χ

Reynolds number scaling of turbulent premixed combustion was explored in a previous works by Kulkarni et al. [1–3] using the same numerical dataset in this paper. The area ratio is expressed as the product of the maximum value of the SDF, Σ_m, the flame brush thickness, δ_T, and a shape factor, β, written as

$$\chi = \Sigma_m \delta_T \beta, \tag{27}$$

$$\beta = \frac{1}{\mathcal{P}_r(r=\tilde{r})\delta_T}\left(\frac{\tilde{r}}{R}\right)^2, \tag{28}$$

where $\tilde{r}$ is the radial location of the peak SDF. The shape factor, β, is related solely to the functional form of the probability density function of the flame location, $\mathcal{P}_r$. It was found that $\mathcal{P}_r$ is well approximated by a normal distribution, parametrized by its mean, R, and standard deviation, $\delta_T/\sqrt{2\pi}$. This allows us to write β as

$$\beta = 0.25\left(1+\sqrt{1-8\alpha^2}\right)^2 \exp\left[\left(\sqrt{1-8\alpha^2}-1\right)^2/8\alpha^2\right], \tag{29}$$

where $\alpha = \delta_T/(\sqrt{2\pi}R)$ is the standard deviation normalized by the mean. The shape factor, β, is a monotonic function of $\alpha = \delta_T/\sqrt{2\pi}R$.

A wrinkling length scale, L^*, is defined based on the peak SDF as $L^* = (4\Sigma_m)^{-1}$ and it was found that the ratio of the integral length scale, l, and the wrinkling scale is approximated by a power law scaling with the Reynolds number,

$$l/L^* \sim \mathrm{Re}_\lambda^{1.13}. \tag{30}$$

This scaling law is shown in Fig. 2a with data from all four flame configurations. We rearrange Eq. (27) and use the above scaling to obtain

$$\chi = \Sigma_m\delta_T\beta = 0.25(l/L^*)(\delta_T/l)\beta = C_\chi \mathrm{Re}_\lambda^\zeta f(s)\beta, \tag{31}$$

where C_χ is a constant, ζ is the Reynolds number exponent, and $f(s)$ captures the dependence of δ_T/l on logarithmic time $s = \log(1+t/t_0)$. The implications of Eq. (31) are significant, in that χ is expressed directly as a power law of the Reynolds number, which varies in time as turbulence decays. The remaining term, $f(s) = \delta_T/l$, was found be approximately the same across configurations, but is fit to individual cases as discussed later. Modeling this term requires solving the evolution equation of the turbulent flame brush thickness, δ_T, but this is beyond the scope of the present work.

The power law decay of the turbulent kinetic energy (Eq. (1)) can be extended to the Taylor microscale Reynolds number as

$$\frac{Re_\lambda}{Re_{\lambda,0}} = \left(1+\frac{t}{t_0}\right)^{-(1-n)/2}\left(\frac{\nu}{\nu_0}\right)^{-1/2}, \tag{32}$$

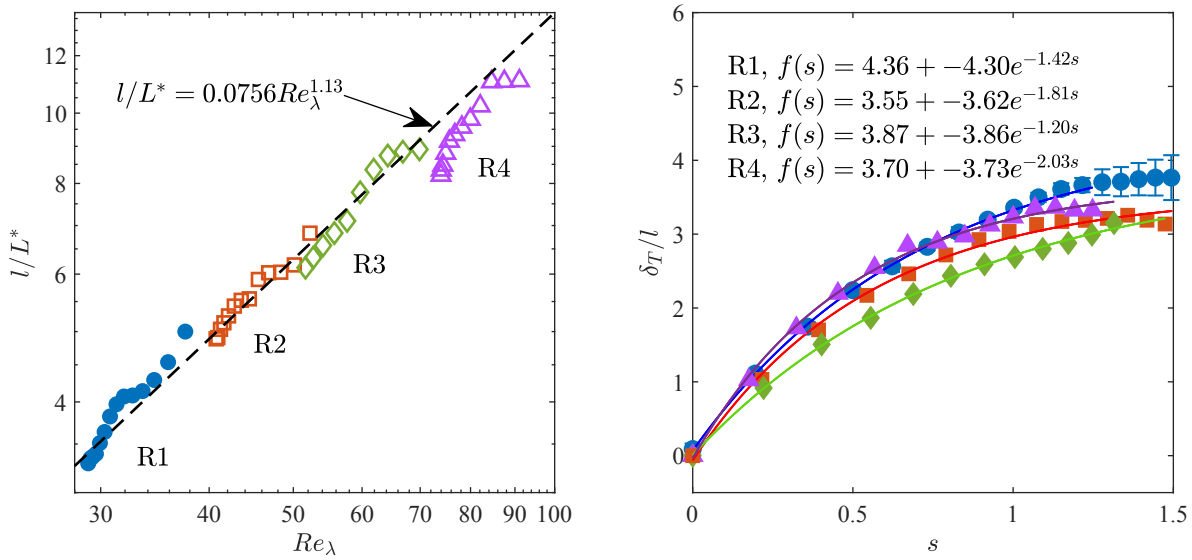

(a) Reynolds scaling of wrinkling length scale **(b) Collapse of $f(s) = \delta_T/l$ across configurations**

Fig. 2 The scaling of (a) l/L^* observed by Kulkarni et al. [1] and (b) approximate collapse of δ_T/l. Also shown in (b) are the exponential fits for $f(s)$ used in the present model.

where ν is the kinematic viscosity of the reactant mixture at time, t. The viscosity ratio, ν/ν_0, can be modeled using Sutherland's law for the dynamic viscosity, μ, and isentropic compression, as

$$\nu/\nu_0 = p^{\frac{3\gamma_u - 1}{2\gamma_u}} \left(\frac{1 + \tilde{T}_S}{p^{\frac{\gamma_u - 1}{\gamma_u}} + \tilde{T}_S} \right), \tag{33}$$

where γ_u is the isentropic expansion coefficient for the reactants, $\tilde{T}_S = T_S/T_{u,0}$ is the Sutherland temperature normalized by the initial reactant temperature. For the range of pressures considered in this work, $\nu/\nu_0 \approx 1$ and can be assumed to be so without loss of accuracy.

For the purposes of the model used in this work, $f(s)$ is obtained through fits of δ_T/l to DNS data using an exponential asymptotic function of the form, $f(s) = a_1 + a_2 \exp(a_3 s)$, as shown in Fig. 2b.

E. Flame Stretch model for $\mathcal{I}$

In the numerical studies described in §II, it was observed that the correction factor, $\mathcal{I}$, was consistently lower than unity across all configurations, as shown in Fig 3a. Moreover, the values of $\mathcal{I}$ appear to approach unity as the flame progresses and are smaller for configurations with smaller initial radii. These observations suggest that this factor may reflect flame stretch effects.

The correction factor is frequently associated to flame stretch effects, and is frequently referred to as the stretch factor. In a previous work [**?**] studying the flame brush evolution in the same numerical data set, it was found that laminar flame stretch theory applied to the mean flame stretch rate components (tangential and normal strain rates) allowed to model the area weighted flame displacement speed, $\langle S \rangle_w$. This provides a strong argument in favor of modeling $\mathcal{I}$ using laminar flame stretch theory. In this work, $\mathcal{I}$ will be henceforth referred to as the stretch factor resulting from our choice of model, and to maintain consistency with the literature.

The Markstein theory [5] for flame stretch effects on laminar steady flames follows the following equation linear in the flame stretch rate, K.

$$\frac{S_L}{S_L{}^0} = 1 - \frac{\mathcal{L}_M}{S_L^0} K = 1 - \mathcal{M} K \tau_L^0, \tag{34}$$

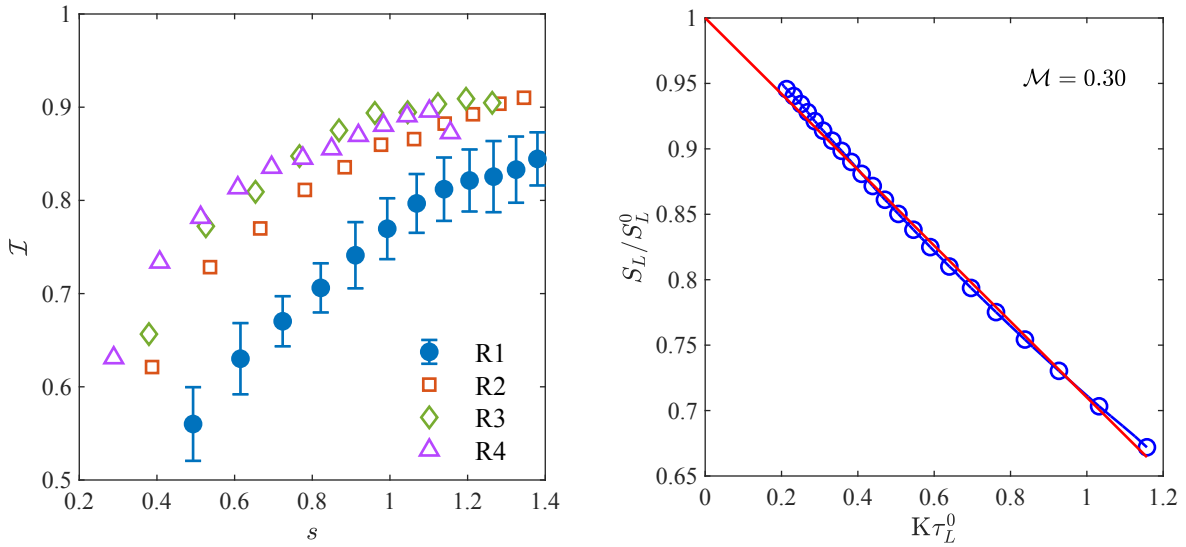

(a) (b)

Fig. 3 (a) The correction factor, $\mathcal{I}$ observed in the DNS plotted against logarithmic time, s, for the 4 DNS configurations and (b) the linear Markstein theory model described in Eq. (34), fit to laminar DNS data for the purpose of calculation of the Markstein number, $\mathcal{M}$, for the mixture under study.

where $\mathcal{L}_M$ is the Markstein length, $\mathcal{M}$ is the Markstein number, defined as $\mathcal{M} = \mathcal{L}_M/\delta_L^0$. The unstretched laminar flame properties S_L^0, τ_L^0 and δ_L^0 are calculated using steady 1D laminar flames at various instantaneous reactant states, characterized by the reactant temperature, T_u, and chamber pressure, p. Specifically, p and T_u are varied assuming isentropic compression of the reactants. In this work, we model $\mathcal{I}$ using Markstein theory for stretch rate effects.

Recall that $\mathcal{I}$ is defined as

$$\mathcal{I} = \frac{\rho^* \langle\!\langle S \rangle\!\rangle_A}{\rho_u S_L^0}. \tag{35}$$

The laminar flame speed, S_L, measured relative the the reactant velocity, is related to the displacement speed as $S_L = \rho^* S/\rho_u$. Using Eq. (35), and substituting the equation for Markstein theory (Eq. (34)) into the definition of $\mathcal{I}$, we obtain

$$\mathcal{I} = 1 - \frac{\mathcal{L}_M}{S_L^0}\langle\!\langle K \rangle\!\rangle_A = 1 - \mathcal{M}\tau_L^0 \langle\!\langle K \rangle\!\rangle_A. \tag{36}$$

The area-weighted mean flame stretch rate is the source term in the evolution equation for the flame SDF, Σ, which reads [21, 22, 27]

$$\frac{\partial \Sigma}{\partial t} + \frac{1}{r^2}\frac{\partial}{\partial r}(\langle u_r + S n_r \rangle_w \Sigma) = \langle K \rangle_w \Sigma, \tag{37}$$

where $u_r = \mathbf{u} \cdot \hat{\mathbf{e}}_r$ and $n_r = \mathbf{n} \cdot \hat{\mathbf{e}}_r$ are the radial components of the velocity and flame surface normal vectors, respectively. The volumetric integral of the above equation reads

$$\iiint_V \frac{\partial \Sigma}{\partial t} dV + \iiint_V \frac{1}{r^2}\frac{\partial}{\partial r}(\langle u_r + S n_r \rangle_w \Sigma) dV = \iiint_V \langle K \rangle_w \Sigma dV. \tag{38}$$

Integrating the terms and using the definition of the global average (Eq. (17)), this simplifies to

$$\frac{dA}{dt} + 4\pi \cancelto{0}{\langle u_r + S n_r \rangle_w \Sigma}\Big]_{r=0}^{\infty} = A \langle\!\langle K \rangle\!\rangle_A. \tag{39}$$

Further, using the definition for χ (Eq. (19)), the global average flame stretch rate is

$$\langle\langle K \rangle\rangle_A = \frac{1}{A}\frac{dA}{dt} = \frac{2}{R}\frac{dR}{dt} + \frac{1}{\chi}\frac{d\chi}{dt}. \tag{40}$$

Equation (36) implies that $\mathcal{I} < 1$ for any $\mathcal{M} > 0$ for an expanding flame with $\langle\langle K \rangle\rangle_A > 0$, so we expect Markstein effects to reduce the area-weighted mean displacement speed. Using the scaling model for χ, and expressing derivatives in s-space, the expression for the stretch factor $\mathcal{I}$ reads

$$\mathcal{I} = 1 - \mathcal{M}C_2\frac{\exp(-s)}{n}\left(\frac{2}{\hat{R}}\frac{d\hat{R}}{ds} + \frac{1}{f(s)}\frac{df(s)}{ds} + \zeta\left(\frac{1-n}{2}\right) + \frac{1}{\beta}\frac{d\beta}{ds}\right), \tag{41}$$

where $C_2 = \tau_L^0/\tau_0$ is a ratio of the laminar flame time scale to the reference time scale (eddy turnover time) and ζ is the exponent of Re_λ in the power law.

The Markstein number for a reactive mixture at a given thermodynamic state can be determined with ease, using experiments or numerical simulations of spherically expanding laminar flames [28]. In this work, spherical laminar flame simulations in the same confined configuration as the turbulent flames were used to obtain the laminar flame speed as a function of the flame stretch rate. The Markstein number is obtained using a least squares fit to Eq. (34) as shown in Fig. 3b, with the constraint that $\mathcal{I} = 1$ at $K = 0$, where $K = (2/R)(dR/dt)$. For the reactant mixture under study, the Markstein number was found to be $\mathcal{M} \approx 0.30$.

F. The ODE system

Equations (25) and (26) form a system of two ODEs in R and p. Terms χ and $\mathcal{I}$ are modeled using Eq. (31) and 41, respectively, hence all terms are closed. There are two limiting forms of the above system of ODEs:

1. Unconfined flame limit

In the limit of an unconfined flame with $R_L \to \infty$, the pressure is constant and the system of ODEs reduces to a single ODE for the mean flame radius,

$$\frac{d\hat{R}}{ds} = \sigma n \exp(s)\chi\mathcal{I}\hat{S}_L^0. \tag{42}$$

2. Laminar flame limit

In the limit of a laminar flame with $\chi = 1$, the system reduces to

$$\frac{dR}{dt} = \sigma\mathcal{I}S_L^0 - \frac{R}{3\gamma_b p}\left(\frac{dp}{dt}\right), \tag{43}$$

$$\frac{dp}{dt} = 3\mathcal{I}\left(\frac{S_L^0}{R_L}\right)\Delta_p^{1/3}\sigma^{2/3}(p-p_i)^{2/3}\left(\frac{p}{p_0}\right)^{1/\gamma_u - 2/3\gamma_b}, \tag{44}$$

with the stretch factor $\mathcal{I}$ closed as

$$\mathcal{I} = 1 - \mathcal{M}\tau_L^0\left(\frac{2}{R}\frac{dR}{dt}\right). \tag{45}$$

IV. Results

The ODEs are integrated numerically in MATLAB using `ode45`, which implements the Dormand-Prince method [29], a seven-stage 4th order accurate Runge-Kutta algorithm with variable time-step sizes. The initial conditions are set equal to those in the DNS for the earliest available time snapshot past $t = 0.5\tau_0$, since the turbulent spherical flame undergoes an initial transient during which the turbulent flame brush establishes.

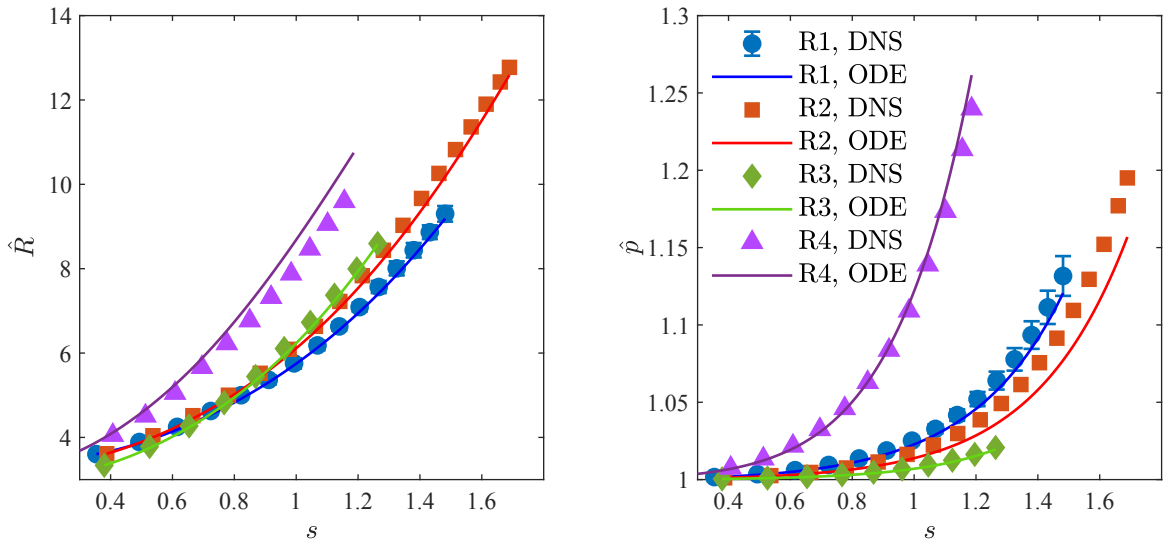

(a) Dimensionless mean flame radius, $\hat{R}$

(b) Dimensionless chamber pressure, $\hat{p}$

Fig. 4 Model solutions (solid lines) for the (a) mean flame radius and (b) chamber pressure compared against corresponding DNS data (symbols).

A. Solutions for R and p

The model solutions for the dimensionless mean flame radius and dimensionless pressure, visualized in Fig. 4, show good agreement with the DNS. There appears to be a slight underestimation of the burning rate at the lower Reynolds numbers and an overestimation in case R4, but these are well within the range of expected statistical variance in these quantities. Specifically in the R1 case, where multiple ensemble runs were performed in order to verify the convergence of statistics through spherical averaging, it is apparent that the predicted pressures and flame radii are within one standard deviation of the mean.

With this functional model, we can test the validity of individual assumptions and study the sensitivity of the solution to system parameters. In the next subsection, we look into the validity of the laminar flame stretch theory applied using mean statistics.

B. Flame Stretch effects

We test the validity of the laminar Markstein model in turbulent flames by comparing the stretch factor calculated directly from DNS using Eq. (35), against estimates from laminar flame stretch theory using Eq. (36). For the latter, the flame stretch rate, K, is calculated directly from DNS data as $K = d \log A/dt$. According to the model proposed in this work, a positive Markstein number implies a stretch factor $\mathcal{I} < 1$, which is consistent with the observations from DNS.

It is found, as plotted in Fig. 5 that under the turbulence conditions in the DNS, laminar flame stretch theory applied to the global average stretch rate is able to provide a very good estimate for the stretch factor, across all configurations. It is also apparent that the same theory, when in our model through Eq. (41), is also able to successfully predict the correction factor observed in the DNS.

The sensitivity of the burning rate on the Markstein number is also explored in Fig. 6, focusing on case R2 ($Re_{\lambda,0} = 59$). The system of ODEs are solved for a range of Markstein numbers and the effects on the mean flame radius and pressure are studied.

We notice a trend of decreasing burning rates characterized by reductions in pressure rise and flame expansion with increasing Markstein number. This is attributed to the mean displacement speed decreasing with Markstein number increasing. This implies a dependence of the correction factor, $\mathcal{I}$ on the Markstein number, across all Reynolds numbers, as shown in Fig. 6. However, the effect of the correction factor itself on dimensionless pressure and dimensionless mean flame radius is quite limited, as the effect of turbulent wrinkling outweighs Markstein effects, especially at higher

Reynolds numbers.

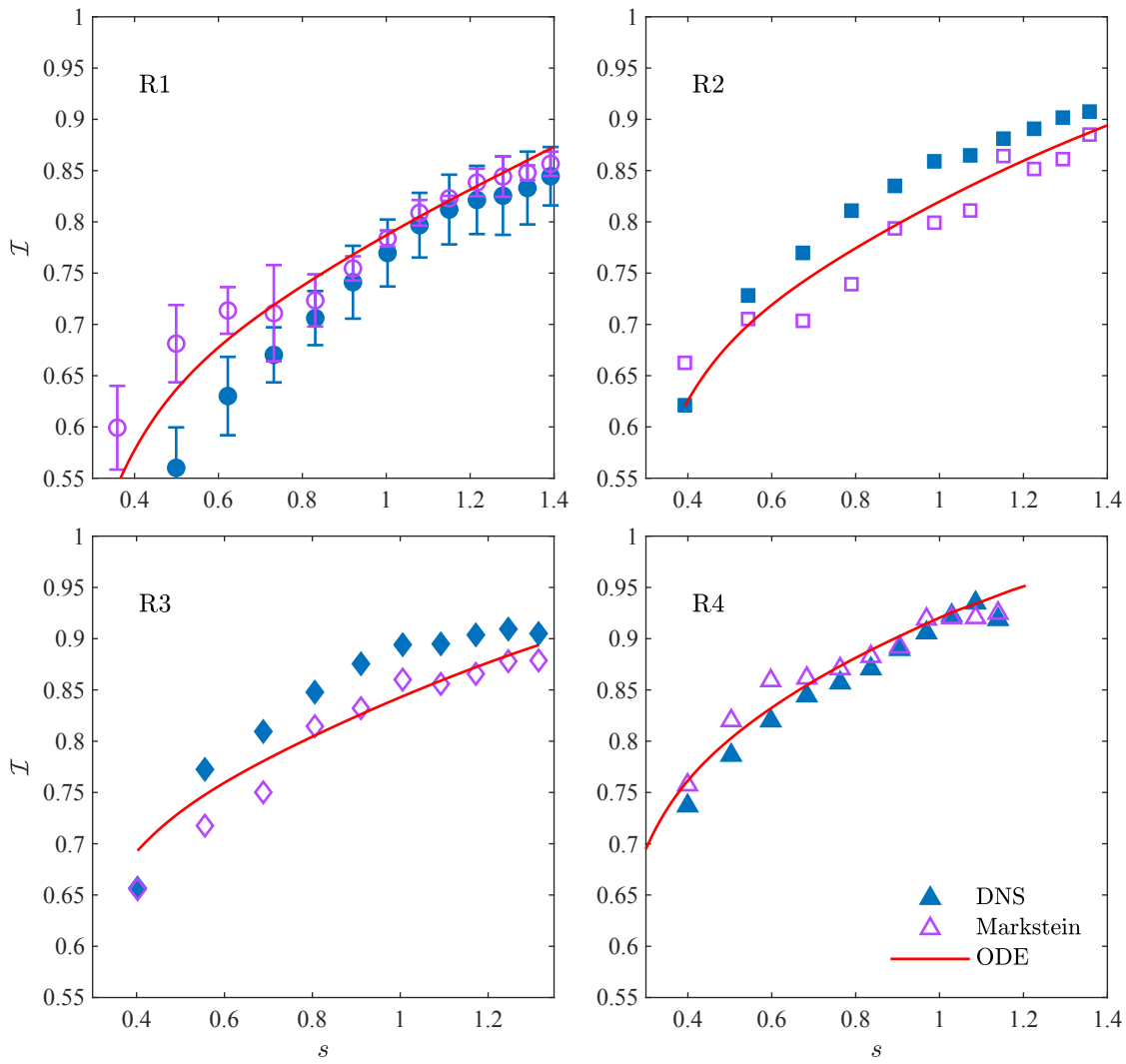

Fig. 5 The stretch factor, calculated from the DNS using Eq. (35) ("DNS") compared against those predicted by laminar flame stretch theory ("Markstein"), given by Eq. (36), along with model solutions ("ODE") plotted across the four DNS configurations.

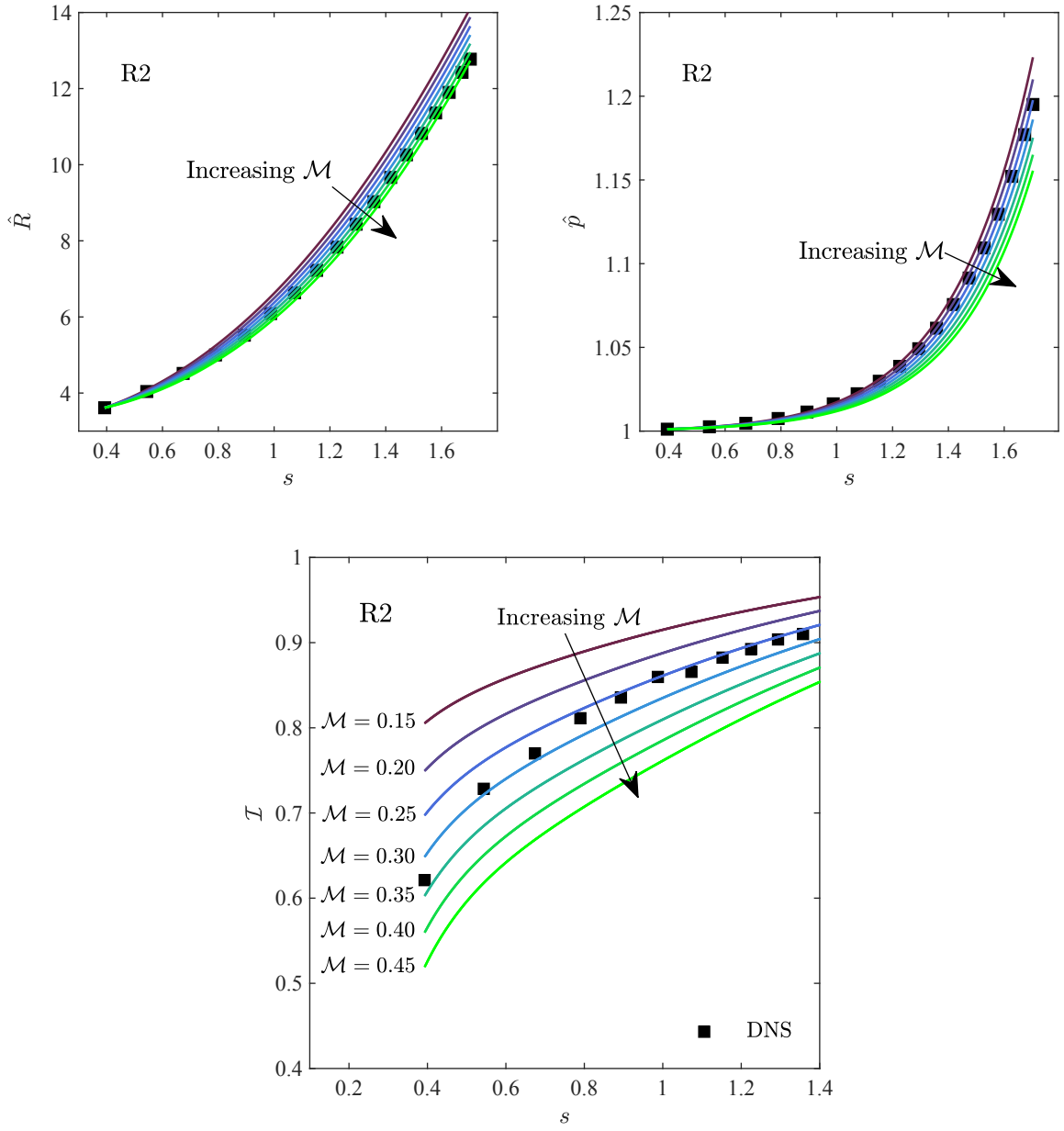

Fig. 6 The solutions from the model (solid lines) for the mean flame radius (top left), pressure (top right) and the stretch factor (bottom) for all for the case R2, solved for a range of increasing Markstein numbers, compared against corresponding DNS data (symbols).

V. Further Work

A closed system of ODEs describing the turbulent flame system would require the modeling of the turbulent brush thickness, δ_T. The ODE for δ_T, as derived and analyzed in Kulkarni and Bisetti [3], reads

$$\frac{d\hat{\delta}_T}{ds} = \underbrace{\frac{3n}{2u'}\frac{2\pi}{\delta_T}\int_0^\infty (r-R)\langle u_r'\rangle_w \mathcal{P}_r dr - \hat{\delta}_T\left(1-\frac{n}{2}\right)}_{\Lambda_1} + \underbrace{\frac{3n}{2u'}\frac{2\pi}{\delta_T}\int_0^\infty (r-R)\overline{u}_r \mathcal{P}_r dr}_{\Lambda_2}$$
$$+ \underbrace{\frac{3n}{2u'}\frac{2\pi}{\delta_T}\int_0^\infty (r-R)\langle Sn_r\rangle_w \mathcal{P}_r dr}_{\Lambda_3} + \underbrace{\frac{3n}{2u'}\frac{2\pi}{\delta_T}\int_0^\infty (r-R)^2\langle K'\rangle_w \mathcal{P}_r dr}_{\Lambda_4}, \quad (46)$$

where u_r is the instantaneous radial velocity, n_r is the instantaneous radial component of the normal to the flame direction, and $K' = K - \langle\langle K\rangle\rangle_A$ is the differential flame stretch rate.

Solution of this ODE requires a closure for the turbulent dispersion of the flame interface (Term Λ_1), which can be modeled using Taylor's theory of Turbulent Dispersion [30, 31]. Additionally, the mean radial velocity field (Term Λ_2) and differential stretch effects (Term Λ_4) also require modeling closures. The effect of the flame propagation (Term Λ_3) on the brush thickness is found to be negligible.

The set of ODEs can be used a create a framework for inferences studies and sensitivity analysis on the Reynolds scaling model, and Markstein theory, using data from DNS and experiments. Experimental work would easily provide high fidelity data for $\tilde{p}$ and $\tilde{R}$. They would also allow the exploration of higher Reynolds numbers than DNS, and would help study the applicability, accuracy and limitations of the Reynolds scaling model proposed under a wider range of thermo-chemical and turbulence conditions.

VI. Conclusions

The burning rate in a spherical turbulent premixed flame was modeled through a set of ordinary differential equations. These equations were derived within the Surface Density Function formalism using observations on flame statistics from large scale Direct Numerical Simulation (DNS) of spherically expanding turbulent premixed flames in homogeneous isotropic turbulence (HIT) across a range of Reynolds numbers.

The data from DNS show that the burning rate enhancement is connected to the increased flame surface area due to turbulent wrinkling along with a correction factor that acts to reduce burning rates slightly. Equations were derived for the chamber pressure and mean flame radius in order to facilitate use when postprocessing experimental data. The equations were expressed in dimensionless form and in logarithmic time consistent with decaying turbulence.

The area ratio was modeled using a Reynolds number scaling hypothesis proposed recently. The correction factor was postulated to be related to flame stretch effects. Laminar flame stretch theory was applied to the turbulent flames using a globally averaged flame speed and stretch rate. The ODEs were integrated with initial conditions from fully developed DNS turbulent flame snapshots, and solutions compared against DNS data. The solutions were found to match the DNS data. Further analysis into the flame stretch model showed that laminar flame stretch theory was able to predict the stretch factor for the flames considered. It is noted that the current system of ODEs is not fully closed, as the flame brush thickness is an input taken from DNS data at this point. Future work in this direction was discussed.

Appendix

A. Approximation of Mean Flame Radius

The mean flame radius, R, as defined in Eq. (4), is the average radial distance of the flame surface, which is equivalent to the area-weighted average of the radial location of the flame, over the domain. We can also define a sphere of volume, V_b, of the products with radius $R_b = (3V_b/4\pi)^{1/3}$. Burnt gases in the domain are identified by $C(\mathbf{x},t) > C^*$, where C^* is a threshold value of C^*. This allows us to write V_b as

$$V_b = \iiint_V H(C-C^*)dV = 4\pi\int_0^\infty r^2\langle H(C-C^*)\rangle dr, \quad (47)$$

where $\langle H(C-C^*)\rangle$ is the ensemble mean of the Heaviside function, and is a function of r and t alone. By definition,

$$\langle H(C-C^*)\rangle = 1(\mathbb{P}(C>C^*;r,t)) + 0(\mathbb{P}(C<C^*;r,t)) = \mathbb{P}(C>C^*;r,t), \tag{48}$$

$$= \int_{C^*}^{1} \mathcal{P}_C(c;r,t)dc. \tag{49}$$

where $\mathbb{P}(\mathcal{C} \in [a,b];r,t)$ is the probability of $\mathcal{C} \in [a,b]$ and $\mathcal{P}_C$ is the PDF of C.
Using the Bray-Moss-Libby model [19, 20], we can express $\mathcal{P}_C$ as

$$\mathcal{P}_C(c;r,t) = \alpha(r,t)\delta(c) + \beta(r,t)\delta(1-c) + \mathcal{F}(r,t)P_f(c;r,t). \tag{50}$$

Using the result above, and assuming a thin flame, i.e. $\mathcal{F} << 1$, we write

$$\langle H(C-C^*)\rangle = \int_{C^*}^{1} [\alpha(r,t)\delta(c) + \beta(r,t)\delta(1-c) + \mathcal{F}(r,t)P_f(c;r,t)]dc \tag{51}$$

$$= \beta(r,t) + \cancelto{\mathcal{O}(\mathcal{F})}{\int_{C^*}^{1} \mathcal{F}(r,t)P_f(c;r,t)dc} \tag{52}$$

We can also write the ensemble mean of the progress variable, C, as

$$\langle C\rangle = \int_{0}^{1} c\mathcal{P}_C(c;r,t)dc \tag{53}$$

$$= \beta(r,t) + \cancelto{\mathcal{O}(\mathcal{F})}{\int_{0}^{1} c\mathcal{F}(r,t)P_f(c;r,t)dc} \tag{54}$$

Hence, under the assumption of a thin flame, $\langle H(C-C^*)\rangle \approx \langle C\rangle$. Further, based on observations, we find that $\langle C\rangle(r,t)$ is well approximated by a complementary Gaussian cumulative distribution function (CDF), stemming from the PDF of the flame location, $\mathcal{P}_r$ being approximately Gaussian, both characterized by a mean, R, and standard deviation, $\delta_T/\sqrt{2\pi}$, i.e.

$$\langle C\rangle = \frac{1}{2}\left[1 - \mathrm{erf}\left(\frac{\sqrt{\pi}(r-R)}{\delta_T}\right)\right]. \tag{55}$$

Substituting the result above, into Eq. (47), we obtain

$$V_b = 2\pi \int_{0}^{\infty} r^2 \left[1 - \mathrm{erf}\left(\frac{\sqrt{\pi}(r-R)}{\delta_T}\right)\right] dr \tag{56}$$

$$= \left(\frac{2\pi R^3}{3} + R^3\hat{\alpha}^2\right)\left[1 - \mathrm{erf}\left(\frac{\sqrt{\pi}}{\hat{\alpha}}\right)\right] + \frac{2R^3}{3}\hat{\alpha}(1+\hat{\alpha}^2)\exp\left(-\frac{\pi}{\hat{\alpha}^2}\right), \tag{57}$$

where $\hat{\alpha} = \delta_T/R$. The volume contained within a sphere of radius equal to the mean flame radius R, is $V_R = \frac{4\pi}{3}R^3$. Also, from Eq. (57), $V_b/V_R = (R_b/R)^3$ is a function of δ_T/R alone, and reads

$$\frac{V_b}{V_R} = \underbrace{\left(\frac{1}{2} + \frac{3}{4\pi}\hat{\alpha}^2\right)\left[1 - \mathrm{erf}\left(\frac{\sqrt{\pi}}{\hat{\alpha}}\right)\right]}_{T_1} + \underbrace{\frac{1}{2\pi}\hat{\alpha}(1+\hat{\alpha}^2)\exp\left(-\frac{\pi}{\hat{\alpha}^2}\right)}_{T_2}, \tag{58}$$

The above expression is plotted against δ_T/R in Fig. 7, and it is clearly seen that $R_b \to R$ as $\delta_T/R \to 0$. In the DNS, we observe a δ_T/R in the range 0.4-0.6.

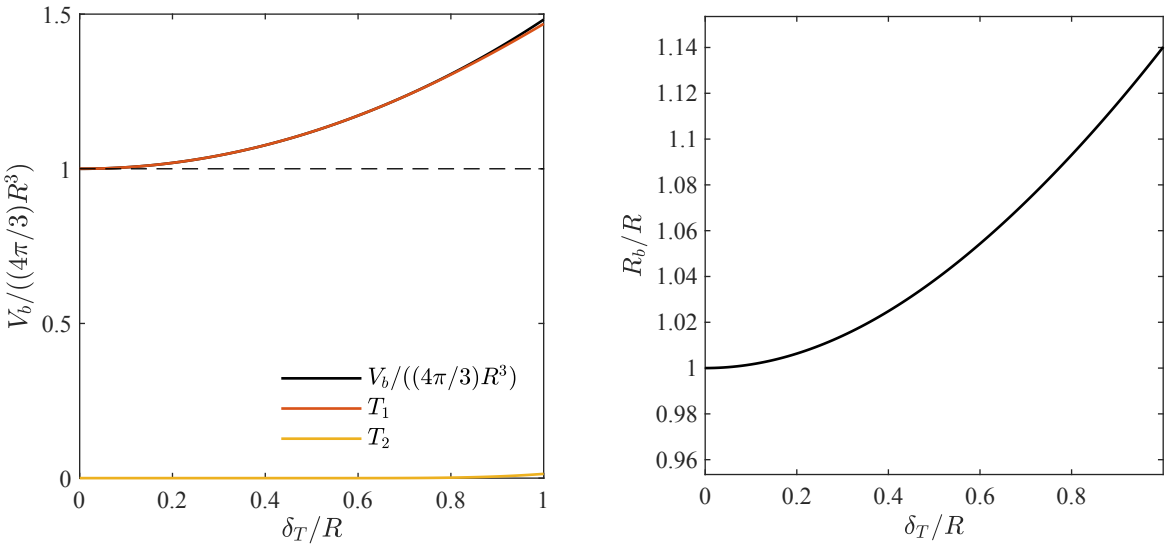

(a) **(b)**

Fig. 7 (a) The ratio of the burnt gas volume to the volume contained within a sphere of mean flame radius, V_b/V_R, and (b) the ratio of the radius of the burnt gas volume to the mean flame radius, R_b/R, both plotted against the ratio of the flame brush thickness to the mean flame radius, δ_T/R, with contributions from individual terms shown for V_b/V_R.

References

[1] Kulkarni, T., Buttay, R., Kasbaoui, M. H., Attili, A., and Bisetti, F., "Reynolds number scaling of burning rates in spherical turbulent premixed flames," *Journal of Fluid Mechanics*, Vol. 906, 2020. https://doi.org/10.1017/jfm.2020.784.

[2] Kulkarni, T., and Bisetti, F., "Surface morphology and inner fractal cutoff scale of spherical turbulent premixed flames in decaying isotropic turbulence," *Proceedings of the Combustion Institute*, Vol. 38, No. 2, 2021, pp. 2861–2868. https://doi.org/10.1016/j.proci.2020.06.117.

[3] Kulkarni, T., and Bisetti, F., "Analysis of the development of the flame brush in turbulent premixed spherical flames," *Combustion and Flame*, Vol. 234, 2021, p. 111640. https://doi.org/10.1016/j.combustflame.2021.111640.

[4] Driscoll, J. F., "Turbulent premixed combustion: Flamelet structure and its effect on turbulent burning velocities," *Progress in Energy and Combustion Science*, Vol. 34, No. 1, 2008, pp. 91–134. https://doi.org/10.1016/j.pecs.2007.04.002.

[5] Markstein, G. H. (ed.), *Nonsteady Flame Propagation*, Vol. 75, Elsevier, 1964. https://doi.org/10.1016/B978-1-4831-9659-6.50001-9.

[6] Clavin, P., and Williams, F. A., "Effects of molecular diffusion and of thermal expansion on the structure and dynamics of premixed flames in turbulent flows of large scale and low intensity," *Journal of Fluid Mechanics*, Vol. 116, 1982, pp. 251–282. https://doi.org/10.1017/S0022112082000457.

[7] Buschmann, A., Dinkelacker, F., Schäfer, T., Schäfer, M., and Wolfrum, J., "Measurement of the instantaneous detailed flame structure in turbulent premixed combustion," *Symposium (International) on Combustion*, Vol. 26, No. 1, 1996, pp. 437–445. https://doi.org/10.1016/S0082-0784(96)80246-3.

[8] Shepherd, I., Cheng, R., Plessing, T., Kortschik, C., and Peters, N., "Premixed flame front structure in intense turbulence," *Proceedings of the Combustion Institute*, Vol. 29, No. 2, 2002, pp. 1833–1840. https://doi.org/10.1016/S1540-7489(02)80222-X.

[9] Im, H. G., and Chen, J. H., "Preferential diffusion effects on the burning rate of interacting turbulent premixed hydrogen-air flames," *Combustion and Flame*, Vol. 131, No. 3, 2002, pp. 246–258. https://doi.org/10.1016/S0010-2180(02)00405-4.

[10] Hawkes, E. R., and Chen, J. H., "Comparison of direct numerical simulation of lean premixed methane–air flames with strained laminar flame calculations," *Combustion and Flame*, Vol. 144, No. 1, 2006, pp. 112–125. https://doi.org/10.1016/j.combustflame.2005.07.002.

[11] Attili, A., Luca, S., Denker, D., Bisetti, F., and Pitsch, H., "Turbulent flame speed and reaction layer thickening in premixed jet flames at constant Karlovitz and increasing Reynolds numbers," *Proceedings of the Combustion Institute*, Vol. 38, No. 2, 2021, pp. 2939–2947. https://doi.org/10.1016/j.proci.2020.06.210, URL https://doi.org/10.1016/j.proci.2020.06.210.

[12] Desjardins, O., Blanquart, G., Balarac, G., and Pitsch, H., "High order conservative finite difference scheme for variable density low Mach number turbulent flows," *Journal of Computational Physics*, Vol. 227, No. 15, 2008, p. 7125–7159.

[13] Smith, G. P., Golden, D. M., Frenklach, M., Moriarty, N. W., Eiteneer, B., Goldenberg, M., Bowman, C. T., Hanson, R. K., Song, S., William C Gardiner, J., Lissianski, V. V., and Qin, Z., "Gri-mech version 3.0," , 1999. URL http://combustion.berkeley.edu/gri-mech/version30/text30.html.

[14] Luca, S., Al-Khateeb, A., Attili, A., and Bisetti, F., "Comprehensive Validation of Skeletal Mechanism for Turbulent Premixed Methane–Air Flame Simulations," *Journal of Propulsion and Power*, Vol. 34, 2018, pp. 153–160. https://doi.org/10.2514/1.B36528.

[15] Peters, N., *Turbulent Combustion*, Cambridge Monographs on Mechanics, Cambridge University Press, 2000. https://doi.org/10.1017/CBO9780511612701.

[16] Batchelor, G. K., and Townsend, A. A., "Decay of isotropic turbulence in the initial period," *Proceedings of the Royal Society of London. Series A. Mathematical and Physical Sciences*, Vol. 193, No. 1035, 1948, pp. 539–558. https://doi.org/10.1098/rspa.1948.0061.

[17] Batchelor, G. K., and Townsend, A. A., "Decay of turbulence in the final period," *Proceedings of the Royal Society of London. Series A. Mathematical and Physical Sciences*, Vol. 194, No. 1039, 1948, pp. 527–543. https://doi.org/10.1098/rspa.1948.0095.

[18] Sinhuber, M., Bodenschatz, E., and Bewley, G. P., "Decay of Turbulence at High Reynolds Numbers," *Phys. Rev. Lett.*, Vol. 114, 2015, p. 034501. https://doi.org/10.1103/PhysRevLett.114.034501.

[19] Bray, K. N., and Moss, J. B., "A unified statistical model of the premixed turbulent flame," *Acta Astronautica*, Vol. 4, No. 3-4, 1977, pp. 291–319. https://doi.org/10.1016/0094-5765(77)90053-4.

[20] Libby, P. A., and Bray, K., "Implications of the laminar flamelet model in premixed turbulent combustion," *Combustion and Flame*, Vol. 39, No. 1, 1980, pp. 33–41. https://doi.org/10.1016/0010-2180(80)90004-8.

[21] Pope, S. B., "The evolution of surfaces in turbulence," *International Journal of Engineering Science*, Vol. 26, No. 5, 1988, pp. 445–469. https://doi.org/10.1016/0020-7225(88)90004-3.

[22] Vervisch, L., Bidaux, E., Bray, K. N. C., and Kollmann, W., "Surface density function in premixed turbulent combustion modeling, similarities between probability density function and flame surface approaches," *Physics of Fluids*, Vol. 7, No. 10, 1995, p. 2496–2503. https://doi.org/10.1063/1.868693.

[23] Chakraborty, N., and Cant, R., "Effects of strain rate and curvature on surface density function transport in turbulent premixed flames in the thin reaction zones regime," *Physics of Fluids*, Vol. 17, 2005. https://doi.org/10.1063/1.1923047.

[24] Lewis, B., and Von Elbe, G., "Determination of the speed of flames and the temperature distribution in a spherical bomb from time-pressure explosion records," *The Journal of Chemical Physics*, Vol. 2, 1934, pp. 283–290. https://doi.org/10.1063/1.1749464.

[25] Luijten, C. C., Doosje, E., and de Goey, L. P., "Accurate analytical models for fractional pressure rise in constant volume combustion," *International Journal of Thermal Sciences*, Vol. 48, No. 6, 2009, pp. 1213–1222. https://doi.org/10.1016/j.ijthermalsci.2008.12.020.

[26] Goodwin, D. G., Speth, R. L., Moffat, H. K., and Weber, B. W., "Cantera: An Object-oriented Software Toolkit for Chemical Kinetics, Thermodynamics, and Transport Processes," https://www.cantera.org, 2021. https://doi.org/10.5281/zenodo.4527812, version 2.5.1.

[27] Trouvé, A., and Poinsot, T., "The evolution equation for the flame surface density in turbulent premixed combustion," *Journal of Fluid Mechanics*, Vol. 278, 1994, p. 1–31. https://doi.org/10.1017/S0022112094003599.

[28] Karpov, V. P., Lipatnikov, A. N., and Wolanski, P., "Finding the markstein number using the measurements of expanding spherical laminar flames," *Combustion and Flame*, Vol. 109, No. 3, 1997, pp. 436–448. https://doi.org/10.1016/S0010-2180(96)00166-6.

[29] Dormand, J., and Prince, P., "A family of embedded Runge-Kutta formulae," *Journal of Computational and Applied Mathematics*, Vol. 6, No. 1, 1980, pp. 19–26. https://doi.org/10.1016/0771-050X(80)90013-3, URL https://www.sciencedirect.com/science/article/pii/0771050X80900133.

[30] Taylor, G. I., "Statistical Theory of Turbulence," *Proceedings of the Royal Society of London. Series A, Mathematical and Physical Sciences*, Vol. 151, No. 873, 1935, pp. 421–444. URL http://www.jstor.org/stable/96557.

[31] Taylor, G. I., "Diffusion by Continuous Movements," *Proceedings of the London Mathematical Society*, Vol. s2-20, No. 1, 1922, pp. 196–212. https://doi.org/10.1112/plms/s2-20.1.196.